

Supporting Information

Enhancing the Toughness of Composites via Dynamic Thiol-Thioester Exchange (TTE) at the Resin-Filler Interface

Nancy Sowan^a, Yinan Lu^b, Kevin J. Kolb^a, Lewis M. Cox^c, Rong Long^b, and Christopher N.

*Bowman^{*a,d}*

^a Materials Science and Engineering Program, University of Colorado, Boulder, CO 80309-0596, USA.

^b Department of Mechanical Engineering, University of Colorado, Boulder, CO, 80309, USA.

^c Mechanical and Industrial Engineering, Montana State University, Bozeman, MT 59717, USA.

^d Department of Chemical and Biological Engineering, University of Colorado, Boulder, CO 80309-0596, USA.

Materials and Methods.

Materials

Pentaerythritol tetrakis(3-mercaptopropionate) (PETMP), Triallyl-1,3,5-triazine-2,4,6-(1H,3H,5H)-trione (TATATO), 1,4-diazabicyclo[2.2.2]octane (DABCO), and propylamine were purchased from Sigma-Aldrich. Irgacure 819 (bis(2,4,6-trimethylbenzoyl)-phenylphosphineoxide) was obtained from BASF. Schott glass (mean particle size 40 nm) untreated were generously donated by Evonik Silicas and used as the inorganic fillers. Prior to implementation and as described later, these fillers were subsequently functionalized with thiol group for inclusion and copolymerization in the composite. All chemicals were used as received. The thioester-diacrylate¹⁸ was synthesized using methods reported elsewhere.

Filler Functionalization

4 g of silica particles (Schott, OX50, 40 nm) were first taken in a glass tube and heated at 165 °C under vacuum using a Buchi heater/condenser for 3 h. The dried nanoparticles were then transferred to a 250 mL bottom rounded flask containing 200 mL of anhydrous toluene

supplemented with 2 g of (3-Mercaptopropyl) trimethoxysilane prereacted for 10 min with 2 g of n-propylamine. The reaction mixture was then refluxed at 120 °C for 24 h. After silanization of nanoparticle, the liquid suspension was centrifuged and the solid pellets were collected thoroughly, and washed with toluene ($3 \times \approx 25$ mL) and methylene chloride ($3 \times \approx 25$ mL) in two separate washing/centrifugation cycles. The washed filler particles were dried under vacuum overnight at 70 °C. Then 2 g of the dried thiol functionalized fillers were reacted with 0.7 g thioester diacrylate in DCM in presence of 3 mL TEA base at R.T overnight. After reaction completion, these nanoparticles were washed with DCM ($1 \times \approx 25$ mL), toluene ($2 \times \approx 25$ mL) and DMSO ($2 \times \approx 25$ mL), and dried under vacuum overnight at 70 °C. The functionalized particles were analyzed by DRIFT FT-IR spectroscopy and TGA. The mass loss difference between silanized and unfunctionalized fillers suggests successful functional group grafting on the surface of glass particles in each case. Also, the DRIFT FT-IR characterization provides evidence of silanol group disappearance around 3745 cm^{-1} and the appearance of the thioester group around 1700 cm^{-1} , implying successful surface modification.

Sample preparation

Mixtures of PETMP, TATATO (1.1:1 molar ratio of thiol:ene), with 1 wt% of I819 as visible light photoinitiator, 2 wt% of DABCO and 10 wt% of SNPs with either the TTE-functionalized adaptive interface or the corresponding control, were prepared. Silanized fillers and resins were blended in a speedmixer (DAC 150 FVZ, Flakteck) to ensure homogenous formulations. Samples were photocured with 400-500 nm visible light at 50 mW/cm^2 for 5 min on each side and then post-cured in an oven at 60 °C for 4 h.

Fourier Transform Infrared Spectroscopy

An FT-IR spectrometer (Nicolet 6700) connected to a tensometer via fiber optic cables was used to monitor the real-time polymerization kinetics in concert with stress measurements. Samples were placed between two cylindrical quartz rods, and 300 mW cm^{-2} light was irradiated from the bottom rod using a light guide connected to a mercury lamp (Acticure 4000, EXFO) with 400–500 nm bandgap filter. The overtone signal of double bonds between $6250\text{--}6096 \text{ cm}^{-1}$ was monitored during the FT-IR measurements.

Polymerization Shrinkage Stress Measurement

Shrinkage stress was measured via a tensometer using cantilever beam deflection theory (American Dental Association Health Foundation, ADAHF-PRC). A composite paste (1 mm in thickness, 6 mm in diameter) was placed between two cylindrical quartz rods, which were previously treated with a methacrylate functional silane to promote bonding at the glass surface/resin interface. A 300 mW cm^{-2} of light was irradiated from the bottom rod using a light guide connected to a mercury lamp (Acticure 4000, EXFO) with a 400–500 nm bandgap filter. Polymerization-induced shrinkage of sample exerted a tensile force which caused the deflection of the aluminum beam. A linear variable differential transformer was used to convert the displacement to shrinkage stress based upon beam calibration constant and cross-sectional area of the sample. For the simultaneous measurement of conversion with shrinkage stress, data were collected continuously for 10 min ($n = 3$).

Thermogravimetric Analysis

TGA (Pyris 1, PerkinElmer) was used to analyze the functionalized silica nanoparticles. Each sample was run in a nitrogen atmosphere (20 mL min^{-1}) from 50 to 850 °C at a heating rate of 10 °C min^{-1} .

Fracture Test

The single edge notch geometry as shown in **Figure 3A** was adopted for the fracture test. The samples were in the form of rectangular thin sheets with width $w = 22\text{mm}$, height $h = 20\text{mm}$ and thickness $t = 0.4 \text{ mm}$. An initial crack with length $a = 5\text{mm}$ was introduced at the edge of the sample by a razor blade. In order to measure the strain field using Digital Image Correlation (DIC), a speckle pattern was applied to the surface of the sample using paint spray (see sample image in **Figure S3** for example). After that the sample was mounted on a mechanical test machine (Instron 5965) for fracture test. The bottom boundary of the sample was fixed, while the top boundary was subjected to a vertical displacement Δ . Although the strain field in the sample is locally non-uniform near the crack, the ratio Δ/h , referred to as the global tensile strain, was used to quantify the loading. The displacement Δ was applied at a constant rate of $\dot{\Delta} = 0.5 \text{ mm/min}$ which corresponds to a global strain rate of $\dot{\Delta}/h = 0.025 \text{ min}^{-1}$. During the test, a video of the sample deformation was recorded using a CCD camera (Canon EOS 6D DSLR along with Canon 100mm F/2.8L Macro Lens).

Digital Image Correlation

Images of the fracture sample during loading were processed by a DIC software NCORR,¹⁹ an open source code written in MATLAB (Mathworks, Natick MA). This software is capable of determining the displacement and strain fields by analyzing the speckle pattern on the sample

between the reference image and the deformed image.²⁰ The reference image was extracted from the initial frame of the video before the displacement loading was applied. The deformed image was extracted from the frames after the displacement loading was applied, and corresponded to a certain global strain Δ/h . Three parameters, i.e., subset radius, subset spacing and strain radius, are required by NCORR to perform DIC, which were set to be 43 pixels, 3 pixels and 10 pixels, respectively, following the documentation of NCORR (<http://www.ncorr.com/>). Note that the images consisted of 1920×1080 pixels and the size of each pixel was 31.2 μm . Through this process, we were able to obtain the displacement and strain fields for the fracture test as shown in **Figure 3** and **Video S1**.

Three-Point-Bending Test

Rectangular bars (2×4×20 mm) and 2 uneven notches (3-mm long notch and 1.5 mm short notch) on one edge were used for three-point bending tests to characterize the fracture behavior. The three-point bending tests were performed using a (MTS 858 Mini Bionix II) testing machines. Five specimens of each composition were tested with displacement rate of 0.75 mm/min.

Tensile Test

Tensile tests were performed using an MTS Exceed E42 universal testing machine with a 500N load cell to obtain the engineering stress–strain curve, the Young’s modulus (determined from the initial linear elastic region of the stress–strain curve), the yield stress (the stress at the maximum), the elongation to break, and the toughness (as measured from the area under the stress–strain curve). Dogbone samples were cut or molded (for brittle specimens) with a 3.15 mm width, 0.1 mm thickness and the gage length was ≈ 15 mm. The specimens were clamped in the grip areas and tested under uniaxial tensile loading at a strain rate of 0.006 min^{-1} .

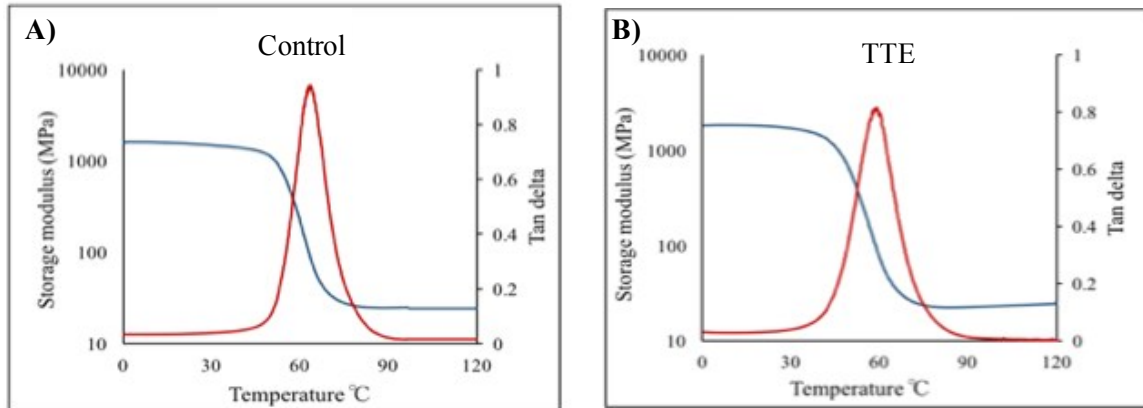


Figure S1. The $\tan \delta$ curves and storage modulus curves of control-based and TTE based composites, obtained from DMTA measurements at 1 Hz.

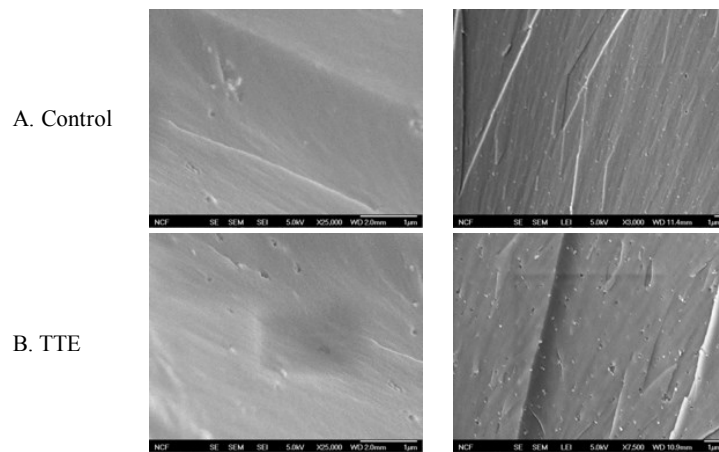


Figure S2. High-resolution scanning electron microscopy (FEG-SEM) images were taken for surfaces of A. control and B. TTE composites.

Table S1. Mechanical properties of both control TTE based composites obtained from tensile testing at 0.0001 s^{-1} displacement rate.

	Tensile strength (MPa)	Elongation at break (%)	Toughness (MJ/m ³)
Control composite	3 ± 0.3	35 ± 4	0.5 ± 0.1
TTE composite	6 ± 1	55 ± 10	1.9 ± 0.4

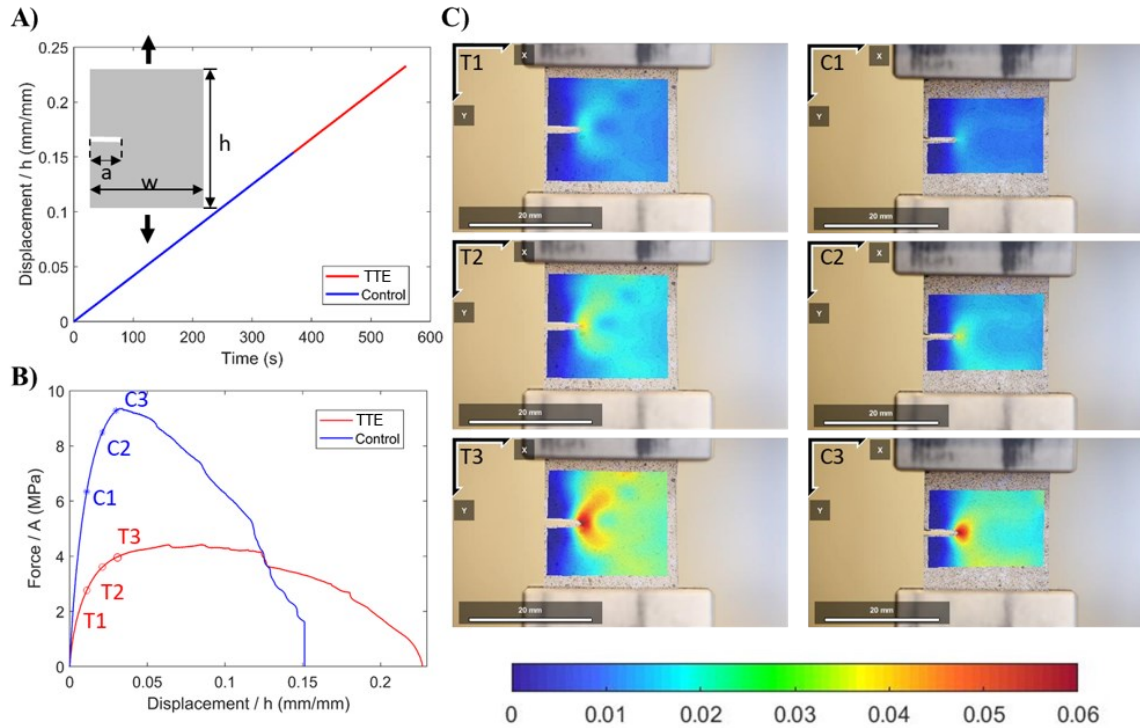


Figure S3. A) Loading history in terms of the global strain Δ/h versus time and B) Nominal tensile stress (force / cross-section area) versus global strain of the single edge notch fracture test using another set of control and TTE-activated samples. C) Spatial distribution of the vertical normal strain components ϵ_{yy} , measured using DIC, at different time frames before crack propagation: T1/C1 (global strain = 1%); T2/C2 (global strain = 2%); T3/C3 (global strain = 3%). Similar to **Figure 3**, the TTE-activated sample also exhibited a more diffusive (i.e., less concentrated) crack tip strain field than the control sample.

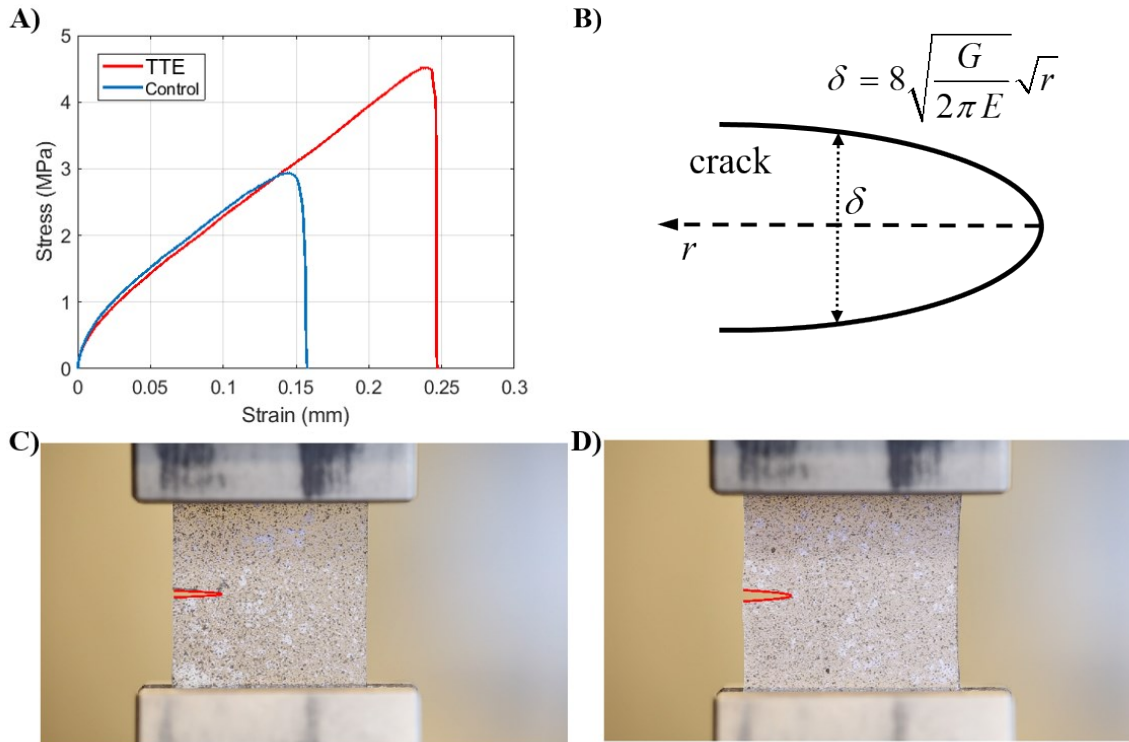


Figure S4. Evaluation of fracture energy G_c based on the crack opening profile. A) Engineering stress-strain curves under uniaxial tension for the control and TTE-activated composites used in the fracture tests as shown in **Figure 3**. The slope of the linear portion was taken as the Young's modulus E , which was 17.3MPa and 18.0MPa for the control and TTE-activated composites, respectively. B) Parabolic crack opening profile for a plane-stress Mode-I crack predicted by the fracture mechanics theory. Fitting of the crack opening profile at the onset of crack propagation for the C) control sample and D) TTE-activated sample. The red lines represent the parabolic fits according to the equation in B), which yielded that $G_c = 260 \text{ J/m}^2$ and 550 J/m^2 for the control and TTE activated samples, respectively.

Video S1. Strain fields in notched TTE and control samples under tension mapped using Digital Image Correlation.

Video S2. Failure of the control 2 notch sample under 3-point bend test at 0.75 mm/min loading rate.

Video S3. Failure of the TTE 2 notch sample under 3-point bend test at 0.75 mm/min loading rate.

Table S2. Mechanical properties of 2-notches samples of both control and TTE based composite under 3-point bend test.

	Maximum stress (MPa)	Elongation at break (%)	Toughness (MJ/m ³)
Control	12 ± 3	10 ± 8	1.9 ± 0.5
TTE	28 ± 6	30 ± 10	6.1 ± 0.9

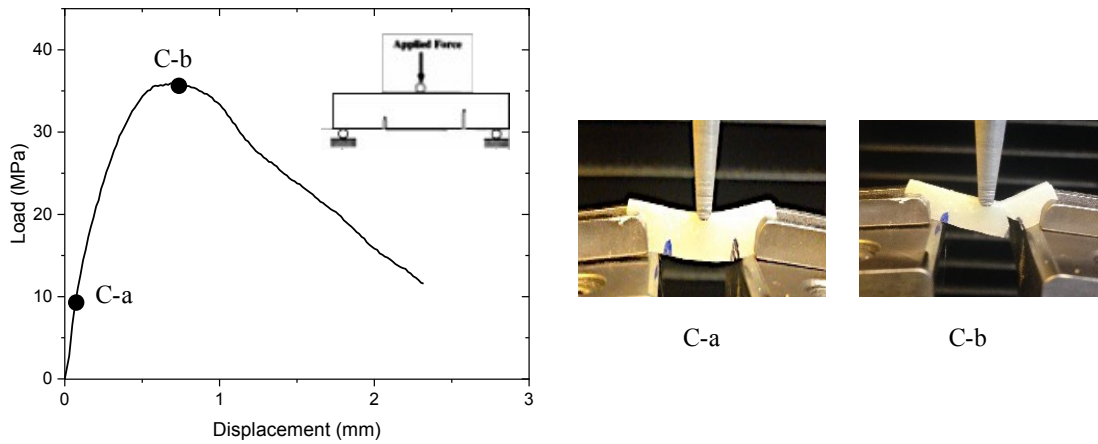


Figure S5. Load-displacement profiles from fracture of double-notched composite specimens and images of the two uneven notches before and after failure at a displacement rate 0.75 mm/min.

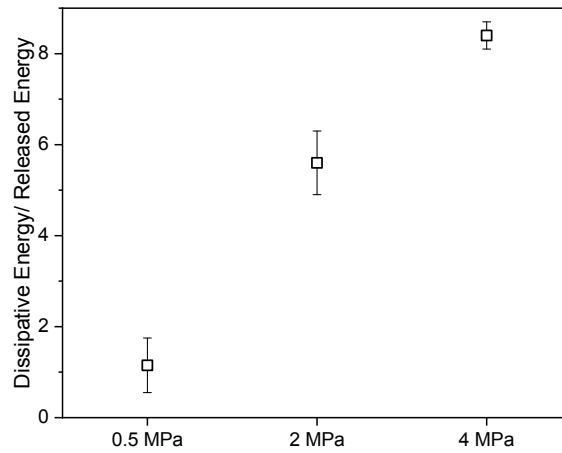


Figure S6. The ratio between the dissipative energy and the released energy of TTE based composites upon applying cyclic loading up to 3 stress level 0.5 MPa, 2 MPa and 4 MPa followed by release of the stress.

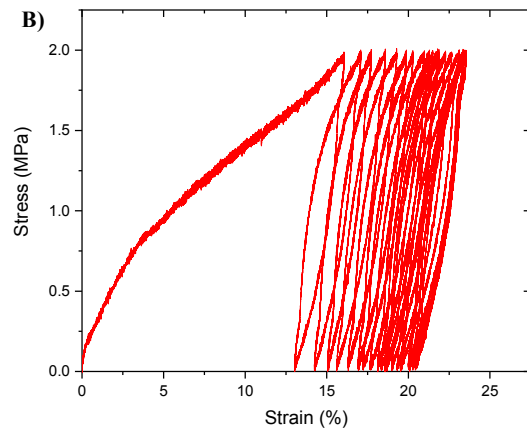
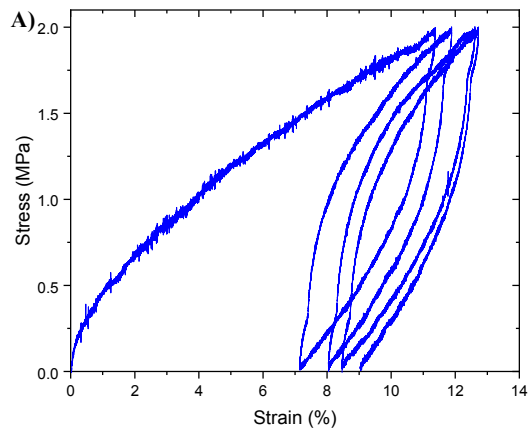


Figure S7. Hysteresis loop cycles during loading of 2 MPa stress then unloading to 0 MPa at 0.1 mm min^{-1} rate for both control and TTE enabled composite.